

DTIC COPY

Plasma Interactions with Spacecraft (I)

V. A. Davis
M. J. Mandell

Science Applications International Corporation
10260 Campus Point Drive
San Diego, CA 92121

Scientific Report No. 2

1 Apr 2009

Approved for public release; distribution unlimited.



AIR FORCE RESEARCH LABORATORY
Space Vehicles Directorate
29 Randolph Road
AIR FORCE MATERIEL COMMAND
HANSCOM AFB, MA 01731-3010

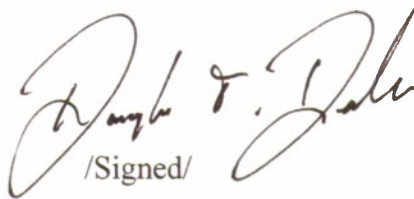
This technical report has been reviewed and is approved for publication.

AFRL-VS-HA-TR-2009-1050 (I)



/Signed/

ADRIAN WHEELOCK
Contract Manager



/Signed/

DWIGHT T. DECKER, Chief
Space Weather Center of Excellence

This report has been reviewed by the ESC Public Affairs Office (PA) and is releasable to the National Technical Information Service (NTIS).

Qualified requestors may obtain additional copies from the Defense Technical Information Center (DTIC). All others should apply to the National Technical Information Service.

If your address has changed, if you wish to be removed from the mailing list, or if the addressee is no longer employed by your organization, please notify AFRL/VSIM, 29 Randolph Rd., Hanscom AFB, MA 01731-3010. This will assist us in maintaining a current mailing list.

Do not return copies of this report unless contractual obligations or notices on a specific document require that it be returned.

Using Government drawings, specifications, or other data included in this document for any purpose other than Government procurement does not in any way obligate the U.S. Government. The fact that the Government formulated or supplied the drawings, specifications, or other data does not license the holder or any other person or corporation; or convey any rights or permission to manufacture, use, or sell any patented invention that may relate to them.

This report is published in the interest of scientific and technical information exchange and its publication does not constitute the Government's approval or disapproval of its ideas or findings.

REPORT DOCUMENTATION PAGEForm Approved
OMB No. 0704-0188

Public reporting burden for this collection of information is estimated to average 1 hour per response, including the time for reviewing instructions, searching existing data sources, gathering and maintaining the data needed, and completing and reviewing this collection of information. Send comments regarding this burden estimate or any other aspect of this collection of information, including suggestions for reducing this burden to Department of Defense, Washington Headquarters Services, Directorate for Information Operations and Reports (0704-0188), 1215 Jefferson Davis Highway, Suite 1204, Arlington, VA 22202-4302. Respondents should be aware that notwithstanding any other provision of law, no person shall be subject to any penalty for failing to comply with a collection of information if it does not display a currently valid OMB control number. **PLEASE DO NOT RETURN YOUR FORM TO THE ABOVE ADDRESS.**

| | | | | | |
|---|------------------------------------|--|-----------------------------------|--|--|
| 1. REPORT DATE (MM-DD-YYYY) 04-01-2009 | | 2. REPORT TYPE Scientific Report No. 2 | | 3. DATES COVERED (From - To) 03-01-2007 to 03-31-2009 | |
| 4. TITLE AND SUBTITLE Plasma Interactions with Spacecraft (I) | | | | 5a. CONTRACT NUMBER FA8718-05-C-0001 | |
| | | | | 5b. GRANT NUMBER | |
| | | | | 5c. PROGRAM ELEMENT NUMBER | |
| 6. AUTHOR(S) V.A. Davis, M.J. Mandell | | | | 5d. PROJECT NUMBER 5021 | |
| | | | | 5e. TASK NUMBER RS | |
| | | | | 5f. WORK UNIT NUMBER A1 | |
| 7. PERFORMING ORGANIZATION NAME(S) AND ADDRESS(ES) Science Applications International Corporation 10260 Campus Point Drive, Mailstop A-2A San Diego, CA 92121 | | | | 8. PERFORMING ORGANIZATION REPORT NUMBER | |
| 9. SPONSORING / MONITORING AGENCY NAME(S) AND ADDRESS(ES) Air Force Research Laboratory 29 Randolph Road Hanscom AFB, MA 01731 | | | | 10. SPONSOR/MONITOR'S ACRONYM(S) AFRL/VSBXR | |
| | | | | 11. SPONSOR/MONITOR'S REPORT NUMBER(S) AFRL-RV-HA-TR-2009-1050 (I) | |
| 12. DISTRIBUTION / AVAILABILITY STATEMENT Approved for public release; distribution unlimited. | | | | | |
| 13. SUPPLEMENTARY NOTES | | | | | |
| <h1>20100315114</h1> | | | | | |
| 14. ABSTRACT The objective of this contract is to develop, incorporate, test, and validate new algorithms for <i>Nascap-2k</i> that are needed to self-consistently compute plasma transport and to model electromagnetic radiation in the near to mid field from VLF (3 kHz to 30 kHz) antennas. The plasma flow models can be used to address various plasma engineering concerns including surface discharges due to meteoroid impact and spacecraft contamination due to electric propulsion plasma plume effects. The goal of this effort is to provide a plasma engineering capability to the spacecraft community. During the third and fourth year of this contract, new database and memory manager software was developed for <i>Nascap-2k</i> , support was provided for the DSX program, and an algorithm was developed for the computation of surface currents on a satellite that is acting as an antenna. Volume II is draft documentation of new software. | | | | | |
| 15. SUBJECT TERMS Nascap-2k, Potentials, Space environment, Spacecraft, Spacecraft charging, DSX, N2kDB | | | | | |
| 16. SECURITY CLASSIFICATION OF: | | | 17. LIMITATION OF ABSTRACT | 18. NUMBER OF PAGES | 19a. NAME OF RESPONSIBLE PERSON |
| a. REPORT UNCLASSIFIED | b. ABSTRACT UNCLASSIFIED | c. THIS PAGE UNCLASSIFIED | | | Adrian Wheelock |
| | | | SAR | 21 | 19b. TELEPHONE NUMBER (include area code) (781) 377-9668 |

CONTENTS

| | | |
|------|--|----|
| 1. | Introduction..... | 1 |
| 1.1. | <i>Nascap-2k</i> | 1 |
| 1.2. | New Database and Memory Manager..... | 2 |
| 1.3. | DSX Calculations..... | 3 |
| 1.4. | Surface Currents..... | 3 |
| 1.5. | DSX Program..... | 3 |
| 1.6. | Contract..... | 4 |
| 1.7. | Publications..... | 4 |
| 2. | Nodal Charge Density..... | 5 |
| 3. | Surface Current Algorithm and Prototype Implementation..... | 7 |
| 3.1. | Objective..... | 7 |
| 3.2. | Algorithm..... | 7 |
| 3.3. | Prototype Implementation..... | 9 |
| 3.4. | Graphics | 10 |
| 3.5. | Example | 10 |
| | Appendix A: <i>Nascap-2k</i> Self-consistent Simulations of a VLF Plasma Antenna | 15 |

FIGURES

| | |
|---|----|
| 1. Nodal Charge Density on $X = 0$ plane using original and revised algorithm for display of extensive quantity. | 6 |
| 2. Nodal Charge Density on $Z = 0$ plane using original and revised algorithm for display of extensive quantity. | 6 |
| 3. The change in charge on a surface element is made up of plasma currents and surface currents. | 8 |
| 4. Iterative calculation of edge currents to obtain surface currents. | 9 |
| 5. Object used for surface current test and development. | 11 |
| 6. Surface current for selected surface elements in the low plasma density case. | 12 |
| 7. Surface current for selected surface elements in the high plasma density case. | 12 |
| 8. Surface currents for the high plasma density case at timestep 7. | 13 |
| 9. Surface currents for the high plasma density case at timestep 12. | 14 |

1. INTRODUCTION

The objective of this contract is to develop, incorporate, test, and validate new algorithms for *Nascap-2k* that are needed to self-consistently compute plasma transport and to model electromagnetic radiation in the near to mid field from VLF (3 kHz to 30 kHz) antennas. The plasma flow models can be used to address various plasma engineering concerns including surface discharges due to meteoroid impact and spacecraft contamination due to electric propulsion plasma plume effects. The goal of this effort is to provide a plasma engineering capability to the spacecraft community.

During the third and fourth year of this contract, new database and memory manager software was developed for *Nascap-2k*, support was provided for the DSX program, and an algorithm was developed for the computation of surface currents on a satellite that is acting as an antenna.

1.1. *Nascap-2k*

During this period, the primary improvement made to *Nascap-2k* was the development of a new database and memory manager system. This is discussed in Section 1.2.

In March 2008, we provided an interim delivery of *Nascap-2k* (version 3.1.3) to AFRL. In January 2009, before incorporation of the new database and memory manager software, we released *Nascap-2k* 3.2 to AFRL and the NASA SEE Program, which distributes the code. Prior to release, we tested the code on our standard suite of problems on Windows and Linux in order to confirm that recent changes had not introduced any problems.

In order to test and develop the multiprocessor capabilities of *Nascap-2k*, we ported the code to a 4 processor Apple Macintosh Pro with the MacOS X.5 operating system with Intel C++ and Fortran compilers. *Nascap-2k* is now fully compatible with the Windows, Red hat LINUX, and MacOS X environments.

We wrote **N2kScriptRunner**, a C++ code that runs a *Nascap-2k* script outside of the Java user interface. Using **N2kScriptRunner**, we compiled, linked, and ran *Nascap-2k* using the OpenMP compiler commands for multiprocessor operations.

We implemented an improvement to the algorithm used to display nodal extensive quantities such as the charge. The approach used is described in Section 2.

In addition to the above, we made a number of small changes to *Nascap-2k*. The most notable are the following:

- We modified the **Results3D** tab of the *Nascap-2k* user interface to allow a user to request that a parameter be displayed on multiple planes at once.

- We added to the **Results** tab the ability to view the surface number of the surface with the minimum and maximum value of the displayed quantity.
- We added to the **Results 3D** tab the ability to view the components of the current.
- We added the Freja environments as default auroral environments on the **Environment** tab.
- We made the specification of an insulating surface as “fixed potential” work properly.
- We removed the use of schema files.
- We added a check to make sure that the particle file filename is no more than 20 characters (the most that can be read by the keyword input routines used by Tracker).
- We added a check to let the user know that there is a missing conductor number.

1.2. New Database and Memory Manager

During the fourth year of this contract, we focused on designing, building, and implementing into *Nascap-2k* the new database and memory management software, **N2kDB**. **N2kDB** is complete and has been incorporated into *Nascap-2k* as an initial implementation. In order to simplify the transition, the initial implementation uses wrappers between the original database commands and the new ones. Thus, in the short term, some of the constraints of the old database remain. Over the next few months, all of the old database commands will be replaced with new ones.

We began by writing a Software Design Document. This document describes the software design, test procedures, and software standards. The document was revised during development as the design matured. This document has subsequently been reorganized into *N2kDB Software Documentation*. This document appears as Volume II of this report.

We developed **N2kDB Test**, a database testbed code. **N2kDB Test** has the same structure as *Nascap-2k* and uses the database in the same manner. It is a small manageable code that we used for testing the database software during development and for developing the proper implementation of the new commands. We anticipate using it intermittently over the next few months; however, we do *not* plan to incorporate it into the released code.

We developed two versions of **N2kDBTool** (console-based and with a Java interface), a stand alone program that reads and writes *Nascap-2k* database files. This program has proved invaluable during development of **N2kDB** and promises to be useful in future *Nascap-2k* development. **N2kDBTool** will be included with future releases of *Nascap-2k*.

N2kDB also includes two testing programs (**msiotest** and **dmtest**) that verify the behavior of the database code itself. They verify that the requested operation is performed correctly. (**N2kDB Test** verifies that the appropriate operation was requested.) These codes will be maintained with **N2kDB**, but will *not* be distributed to users.

N2kDB satisfies all the requirements specified in the Software requirements document. A review of how these requirements are satisfied is given in an appendix to *N2kDB Software Documentation*.

Before incorporation of **N2kDB** into *Nascap-2k*, we released *Nascap-2k* 3.2.

1.3. DSX Calculations

We used *Nascap-2k* to perform a set of self-consistent calculations of the plasma response to a high voltage square wave VLF antenna using the capabilities implemented earlier and described in the previous interim report for this contract. These calculations are included in a paper prepared for the Spacecraft Charging Technology Conference and are the first full test of all of the new capabilities. This paper (M.J. Mandell, V.A. Davis, D.L. Cooke, A.T. Wheelock, C.J. Roth, *Nascap-2k* Self-consistent Simulations of a VLF Plasma Antenna, *Spacecraft Charging Technology Conference*, Biarritz, France, June 2007) is included in Appendix A. We learned that the inclusion of a representation of the thermal distribution at the boundary can influence the current collected by the antenna arms.

1.4. Surface Currents

We are developing a technique for the evaluation of surface currents for DSX and prototyped it in Java. A description of the algorithm and the prototype implementation is in Section 3.

1.5. DSX Program

We supported the DSX program by assuming an active role in the Y-boom high voltage isolation design. To that end, Dr. Myron J. Mandell participated in the following teleconferences and meetings.

- Weekly teleconferences with Y Antenna supplier (L'Garde) from November 6, 2007 to through February 13, 2008.
- A visit to the L'Garde facility to discuss the design issues on November 7, 2007.
- Y Antenna Isolation teleconference on December 19, 2007.
- Weekly teleconferences with the alternate supplier of Y Antenna (ATK) from January 15 to February 25, 2008.
- ATK Isolation face-to-face at Houston Airport (IAH) on February 13, 2008.
- DSX Alternative Y Antenna CDR, Goleta, California on February 26 by teleconference.
- DSX Y Antenna CDR at L'Garde, Tustin, California on February 27.

Dr. Myron Mandell attended and made a presentation at the Workshop on The Remediation of Enhanced Radiation Belts in Lake Arrowhead, California on March 3-6, 2008.

Dr. Mandell also attended the DSX System CDR, Breckenridge, Colorado, May 6-8, 2008.

Dr. Mandell attended the MURI Review and RBR Workshop at Stanford in Palo Alto, California, February 18-19, 2009.

1.6. Contract

The scientists and other researchers who contributed to this work are as follows: Dr. Myron J. Mandell, Dr. Victoria A. Davis, Ms. Barbara M. Gardner, Ms. Katherine Wilcox, Ms. Alisa J. Ward, and Mr. Nicholas R. Baker.

This contract is a follow-on to work performed under earlier contracts: F19628-91-C-0187, Space System-Environment Interactions Investigation; F19628-93-C-0050, Modeling and Post Mission Data Analysis; F19628-89-C-0032, Analysis of Dynamical Plasma Interactions with High Voltage Spacecraft; and F19628-98-C-0074, Spacecraft Potential Control. NASA supported related work under contracts NAS8-98220 and NAS8-02028.

1.7. Publications

The following publications were supported in total or in part by this contract during the third and fourth years.

M.J. Mandell, V.A. Davis, D.L. Cooke, A.T. Wheelock, C.J. Roth, *Nascap-2k Self-consistent Simulations of a VLF Plasma Antenna, Spacecraft Charging Technology Conference, Biarritz, France, June 2007.*

M.J. Mandell, V.A. Davis, E.J. Pencil, M.J. Patterson, H.K. McEwen, J.E. Foster, J.S. Snyder, Modeling the NEXT Multi-Thruster Array Test with *Nascap-2k, Spacecraft Charging Technology Conference, Biarritz, France, June 2007.* (Original research supported by NASA.)

M.J. Mandell, V.A. Davis, E.J. Pencil, M.J. Patterson, H.K. McEwen, J.E. Foster, J.S. Snyder, Modeling the NEXT Multi-Thruster Array Test with *Nascap-2k, IEEE Transactions on Plasma Science, 36*, p. 2309, 2008. (Original research supported by NASA.)

M.J. Mandell, V.A. Davis, A. Wheelock, D.L. Cooke, Modeling Space Weather Effects using *Nascap-2k, GOMACTech-08, Las Vegas, NV, March 2008.*

2. NODAL CHARGE DENSITY

Using an earlier version of *Nascap-2k*, attempts were made to plot the value of the Nodal Charge Density along a line. The plots had non-physical structures, particularly near grid boundaries. Also, the Nodal Charge Density on a plane as displayed on the 3-D Results tab showed non-physical values along grid boundaries. The reason for the non-physical values is that the Nodal Charge Density as displayed is actually the charge on each node as stored in the database and used in the calculations (an extensive quantity) converted to the charge density (an intensive quantity) for the purpose of display. Extensive quantities exist only on nodes, and therefore it does not make sense to discuss their value at an arbitrary point. The correct way to convert an extensive quantity to an intensive quantity is essentially to multiply by the inverse of the volume matrix. Unfortunately, while straightforward, implementing this is quite complex. With a moderate level of effort we were able to implement an improvement to the display of nodal extensive quantities. The approach used is as follows:

- In order to usefully display an extensive quantity, it is necessary to convert it to an intensive quantity.
- Previously, the conversion was done by dividing the value at each node by the cube of the mesh unit. This would be correct, if there were only one grid (except at the outer boundary and near the object).
- We added two grid interface operations to the cut plane display routines. One grid interface operation is before and one after the division of each node by mesh volume. In the first grid interface operation, the extensive quantity on nodes on grid boundaries is transferred from the inner grid to the outer grid. In the second, the intensive quantity (resulting from the division by volume) is shared from the outer grid to the inner grid. No adjustment is made to account for the fact that the appropriate volume for grid interface nodes and those near the object is not the mesh unit cubed.

The nodal charge density, derived from the nodal charge using the old and new approaches for display is shown on the following figures for the moving sphere problem provided as an example. Most of the artificial structures on the grid boundaries have been eliminated.

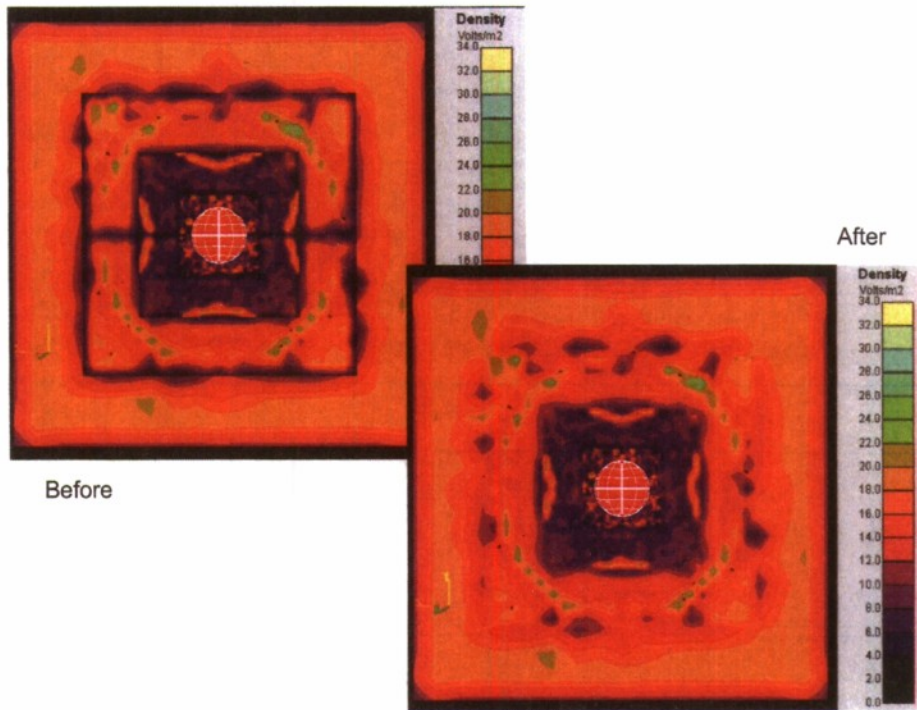


Figure 1. Nodal Charge Density on $X = 0$ plane using original and revised algorithm for display of extensive quantity.

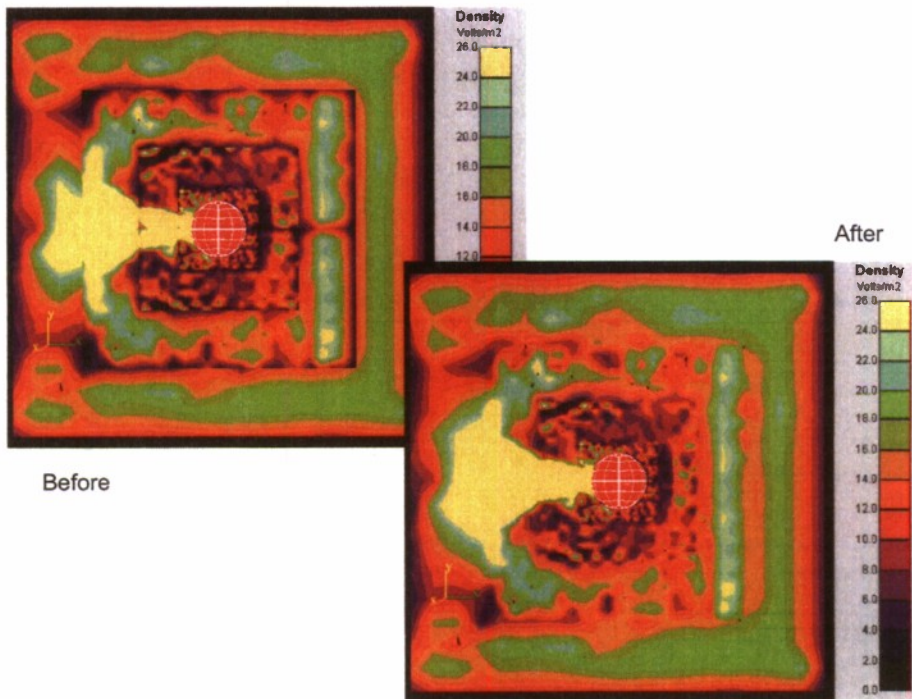


Figure 2. Nodal Charge Density on $Z = 0$ plane using original and revised algorithm for display of extensive quantity.

3. SURFACE CURRENT ALGORITHM AND PROTOTYPE IMPLEMENTATION

3.1. Objective

The objective of the project is to calculate surface currents on a satellite that is acting as an antenna. The satellite has two or more antenna elements (represented by conductor numbers) that are biased in a programmed way by an amplifier, and typically will have passive elements as well. The amplifier injects current at a specified location on each antenna element in order to maintain the programmed voltage. The injected currents, along with plasma currents resulting from the voltage application, flow on the spacecraft surface. These currents are the source of radiated electromagnetic fields.

The plan is to add to *Nascap-2k* the capability to compute these radiated electromagnetic fields. *Nascap-2k* divides spacecraft surfaces into surface elements. The fields could be computed by adding the contributions from the current elements (vectors) for each surface element. The current element for each surface would be the average surface current density times the element area and located at the element centroid.

We have developed an algorithm to calculate these surface currents and are creating a prototype implementation in Java prior to incorporation into *Nascap-2k*.

3.2. Algorithm

Each antenna or passive element is represented by a number of surface elements with a common conductor number. The amplifier provides the charge needed (calculated based on the change in electric field and the plasma currents) to achieve the specified potential change of the conductor during the time step. This charge is injected into a specified surface element and can then flow across the element edges into neighboring surface elements. For surface elements other than the injection element, the change in the charge on the element must equal the sum of the plasma currents and the surface currents crossing its edges, as shown in Figure 3. The current crossing each edge is iteratively computed (as described below). The element surface current (the average current on the element) is the current that best matches the edge currents. This process is performed separately for each conductor. Current is not allowed to flow across an edge separating two different conductors.

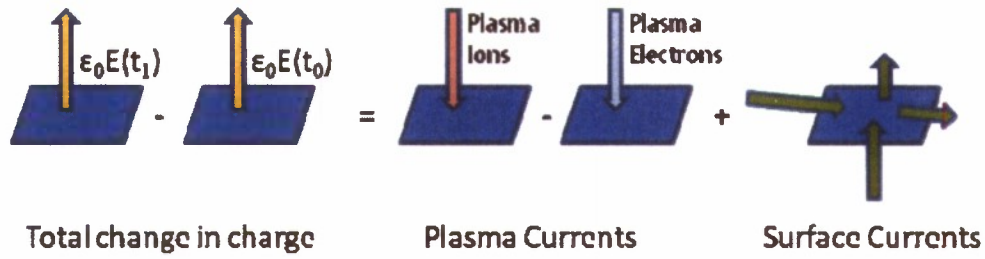


Figure 3. The change in charge on a surface element is made up of plasma currents and surface currents.

Figure 4 shows the steps in this process. The injection current for each conductor is determined by summing over all the surface elements of the conductor. The edge currents are initialized by each element contributing the appropriate portion of its required rate of change in charge. The edge currents are then adjusted until the net current to each surface element is as required. At the beginning of the “Augment Edge Currents” step, we know the discrepancy, ΔI_{elem} , between the amount of current leaving the element across its edges and the amount of current required. The current crossing each edge of the element is augmented by

$$\Delta I_{\text{edge}} = r \Delta I_{\text{elem}} \frac{\ell}{L}$$

where ℓ is the length of the edge, L is the total length of edges bounding the element, and r is a relaxation factor currently set to 0.8. Each non-bounding edge also receives a contribution from its neighboring element. In our experience thus far, the process converges robustly.

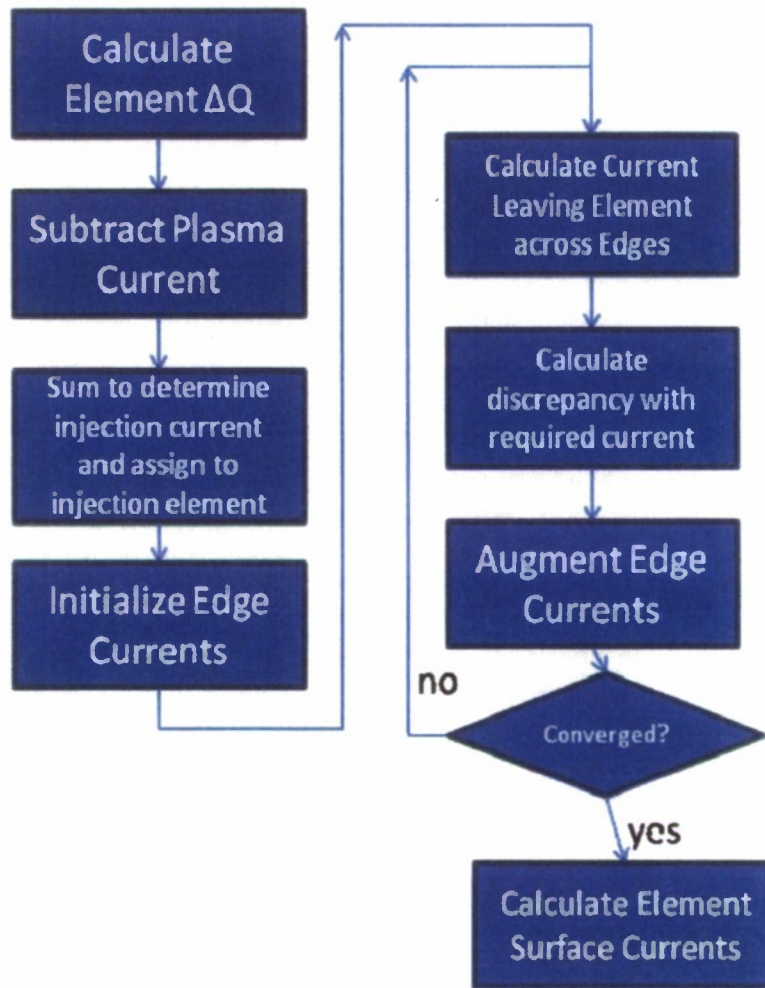


Figure 4. Iterative calculation of edge currents to obtain surface currents.

This algorithm requires the following quantities:

1. The surface elements, including specification of the injection element for each conductor.
2. The rate of change of external electric field for each element.
3. The plasma current to each surface element.
4. The change in charge to be supplied by surface current is $\frac{\epsilon_0 dE}{dt}$ less the plasma current.

3.3. Prototype Implementation

The prototype is pure Java, most of which is derived from existing *Nascap-2k* interface coding. Most of the work is done by the SurfaceCurrents class, with inputs supplied by the two auxiliary classes DEbyDT and PlasmaCurrents. The code relies

heavily on existing ObjectToolkit classes, notably Mesh, Element, and their dependencies. Non-intrusive modifications have been made to Element (e.g., to store the surface currents and to register the injection surface element) and to Mesh (e.g., for graphic display of surface currents).

The code reads in the object mesh and separates it into separate meshes (by conductor). At completion the surface current density is entered into each element of the original mesh (as a Vector3). Current elements, which could be summed to calculate the vector potential, are given by the surface current density times the element area.

$$\Delta I_{\text{edge}} = r \Delta I_{\text{elem}} \frac{\ell}{L} \ell L$$

where ℓ is the total length of edges bounding the element. r is the rate of change of external electric field for each element is computed by a class DEbyDT. Presently DEbyDT reads the .POTS file from a previous *Nascap-2k* calculation using the recently developed N2kDBTool.dll, and differences the stored electric field at adjacent timesteps. The use of actual time step times is not yet implemented.

The plasma current to each surface element is computed by the class PlasmaCurrents. Presently, the plasma current is calculated by a clsEnvironment using the surface element potential.

3.4. Graphics

The surface current (if it exists) for each element is displayed using a Java3D primitive Cone object. The height of the Cone is proportional to the square root of the surface current density and to the square root of the surface element area. As output, the code converts the entire object to a primitive and writes it out along with the element surface currents. The primitive can then be displayed by Object Toolkit. The same display code should work in *Nascap-2k* if the surface elements appear in the mesh that is plotted.

3.5. Example

For development, we used a test object consisting of two adjacent cubes (conductors 1 and 2) as shown in Figure 5. The center surface elements on either end (shown as Gold) are flagged as injection surface elements (to which the bias currents are supplied). During initial development, hard-wired $\frac{dE}{dt}$ values were applied, and alternate injection locations were used to demonstrate that the process converges to sensible results for asymmetric cases.

For this example, a *Nascap-2k* run was performed starting with conductor 1 at 0V and conductor 2 at -1000V, and the bias varied sinusoidally at 10 kHz for 20 timesteps of 5 microseconds each (making one full period). The surface currents application was then

run for two cases, and the output saved at each timestep. We then recorded the time development of surface current at surface elements 78 and 31, as shown in Figure 5.

The two cases were: (a) a small amount of plasma current 180° out of phase with the applied voltage; and (b) plasma current comparable to the $\frac{\epsilon_0 dE}{dt}$ current. For case (a) we expect the surface currents for the two surface elements to be nearly identical, as current is injected into one conductor and leaves the other conductor in a sinusoidal pattern, 90° out of phase with the applied voltage. For case (b) we expect the two surface currents to be different and phase shifted, as the plasma current is always outwardly directed (from the center of the object toward the injection points), so that it adds to one while subtracting from the other.

Figure 6 shows the surface currents for the two selected surface elements in the low plasma density case(a). The small amount of plasma current causes the two curves to be slightly separated, and results in a phase shift of about 15 degrees, as indicated by the accompanying sine wave.

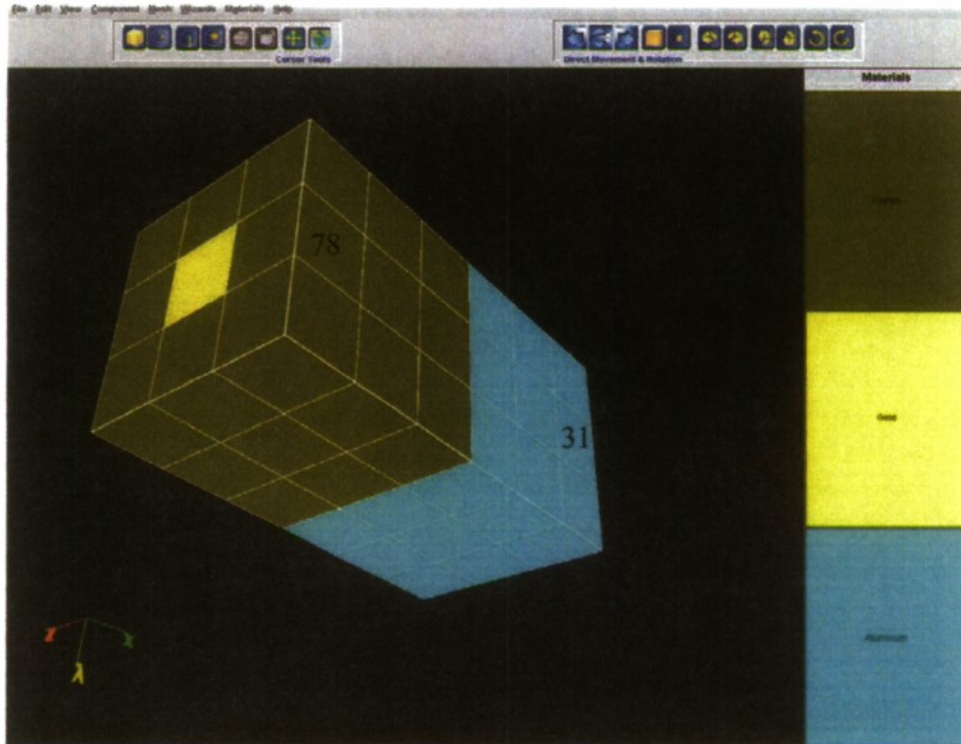


Figure 5. Object used for surface current test and development.

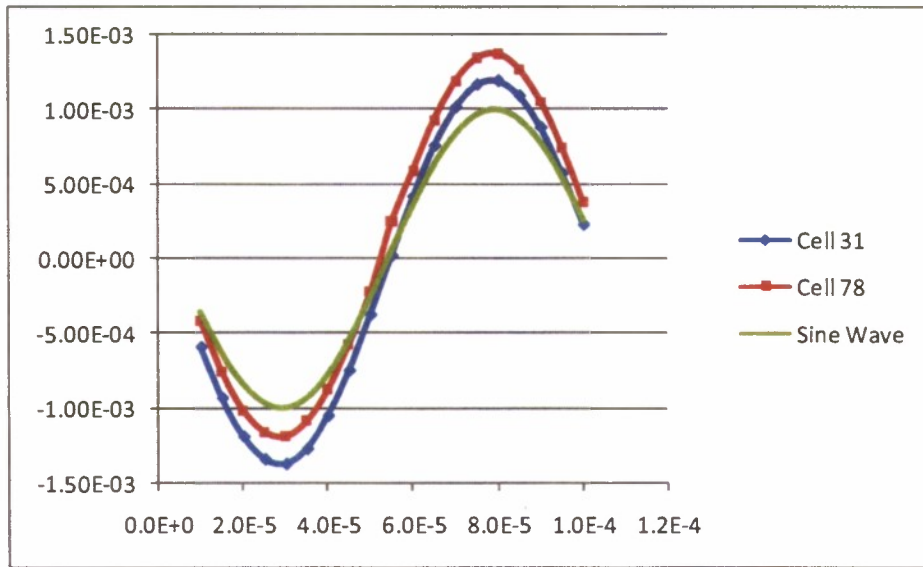


Figure 6. Surface current for selected surface elements in the low plasma density case.

Figure 7 shows the surface currents for the two selected surface elements in the high plasma density case(b). The significant amount of plasma current causes the two curves to be substantially separated, and results in a phase shift of about 45 degrees. The glitches seen near 50 microseconds for surface element 78 and near 100 microseconds for surface element 31 results from electron plasma current collected when the surface elements are near zero potential.

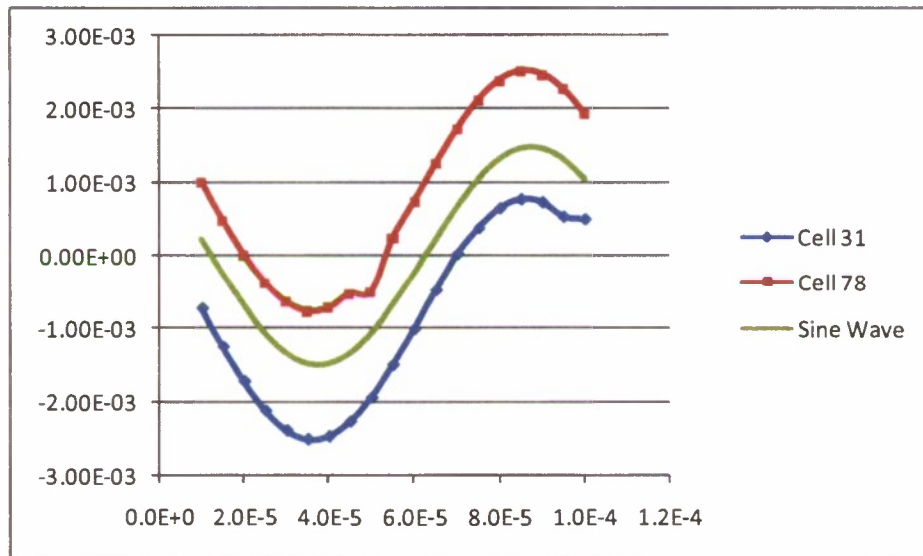


Figure 7. Surface current for selected surface elements in the high plasma density case.

Figure 8 shows surface currents for the high density case at timestep 7, near the maximum in $\frac{dE}{dt}$. At this time all surface currents are in the same direction, and would be of similar magnitude for the two conductors if the plasma current were not significant. Figure 9 shows the surface currents for the same case near a null in $\frac{dE}{dt}$. The surface currents are now due solely to the plasma currents, and flow in opposite directions on the two conductors.

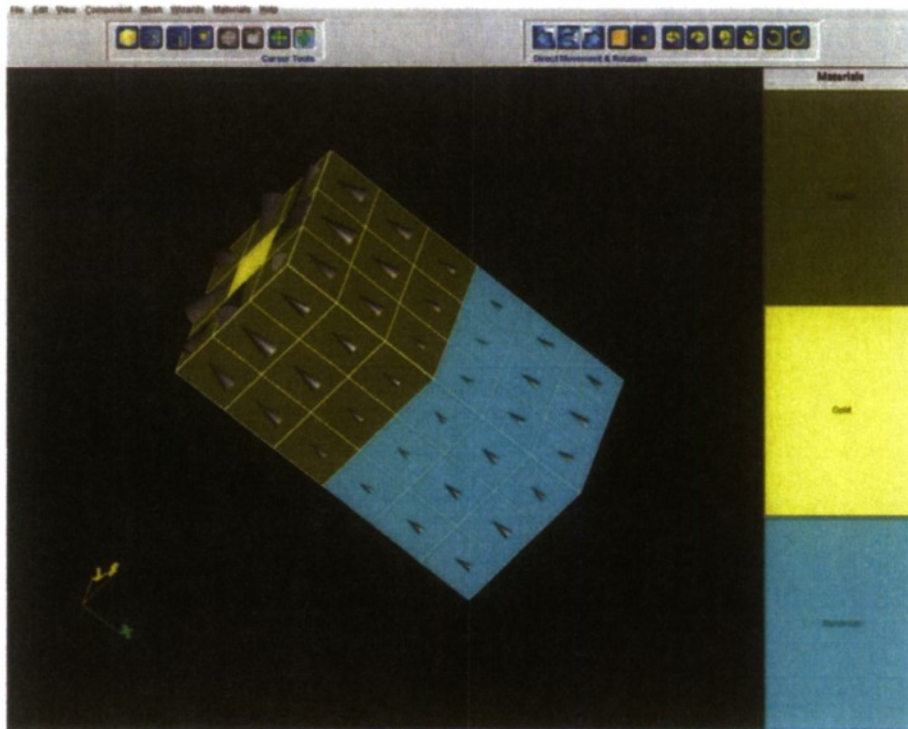


Figure 8. Surface currents for the high plasma density case at timestep 7.

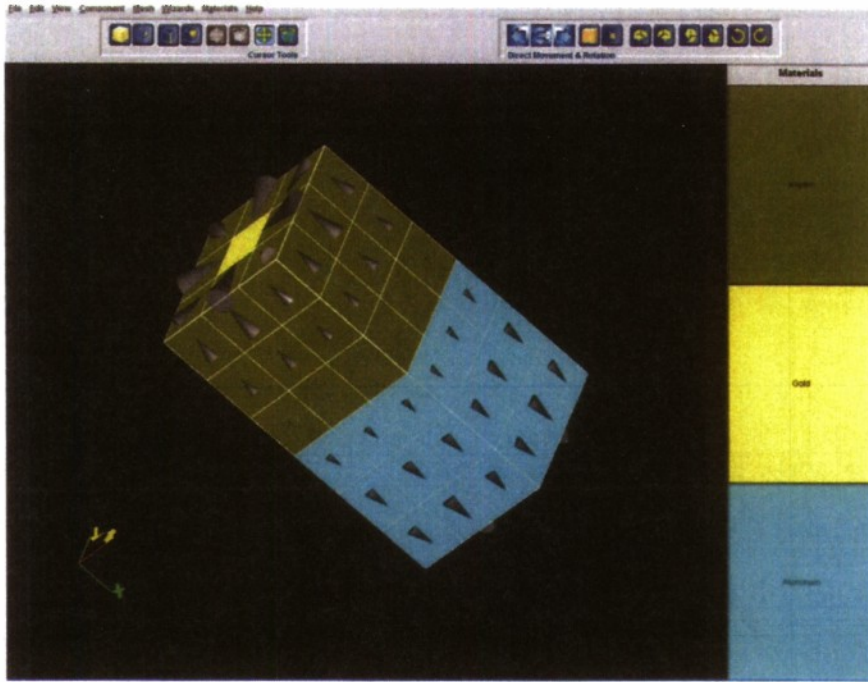


Figure 9. Surface currents for the high plasma density case at timestep 12.

APPENDIX A: *NASCAP-2K* SELF-CONSISTENT SIMULATIONS OF A VLF PLASMA ANTENNA

The following paper was presented at the Spacecraft Charging Technology Conference, Biarritz, France in June 2007.

NASCAP-2K SELF-CONSISTENT SIMULATIONS OF A VLF PLASMA ANTENNA

M. J. MANDELL and V.A. DAVIS

*Science Applications International Corporation
10260 Campus Point Dr., M.S. A1A, San Diego, CA, 92121*

D. L. COOKE and A.T. WHEELLOCK

*Space Vehicles Directorate
Air Force Research Laboratory/VSBX
Hanscom AFB, MA, 01731-3010*

C. J. ROTH

*Atmospheric and Environmental Research Inc.
131 Hartwell Ave., Lexington MA, 02421-3126*

ABSTRACT: *We simulate the plasma response to high voltage square wave VLF antenna in Medium Earth Orbit plasma with Nascap-2k. The plasma is modeled with a hybrid Particle-in-cell (PIC) approach with PIC ions and fluid barometric electron densities. The plasma response, collected ion currents, and chassis floating potential are computed self-consistently with a near-square-wave bias applied to the antennas. Particle injection and splitting are used to replenish the plasma depleted at the boundary, represent the thermal distribution, and maintain appropriately sized macroparticles. Therefore, current limitation due to the thermal distribution of ions and the resulting angular momentum barrier are included. Above the ion plasma frequency the plasma current lags the voltage by about 10° , while below the ion plasma frequency the current leads the voltage by about 7° .*

1 - INTRODUCTION

The response of a plasma to very low frequency (VLF) (3 kHz to 20 kHz) high-voltage antennas at orbital altitudes of 1000 to 10,000 kilometers has been a subject of scientific interest for many decades.^{1,2,3} Plasma waves from VLF antennas with such frequencies ("whistler" waves) are thought to interact with MeV radiation belt electrons. As this antenna frequency is less than both the electron plasma frequency and the electron gyrofrequency (both nearly 300 kHz for a plasma density of 10^9 m^{-3} and a magnetic field of 0.1 gauss), only certain modes can propagate as electromagnetic waves, and the near field is dominated by electrostatic effects. Although a comprehensive self-consistent electromagnetic-electrostatic simulation would be the desired goal, there are many computational challenges to be overcome, so we begin with electrostatic simulations in order to sort out the dominant plasmadynamic effects.

A VLF dipole antenna has two elements, each several centimeters in diameter and many meters long. Due to the ease of electron collection by positive objects, the positive element is at near zero or small positive potential relative to the ambient ionosphere, while nearly the full applied potential appears on the negative element. Because the frequencies of interest are comparable to the ion plasma frequency, the sheath structure is at some intermediate state between the “ion matrix” or “frozen ion” limit (which assumes the ions are stationary and contribute ambient ion density to the space charge) and the equilibrium space charge limit (in which the ions assume a steady-state space charge limited distribution of charge and current). Thus, calculation of the sheath structure and of the ion collection by the antenna requires dynamic (specifically, particle-in-cell, PIC) treatment, at least for the ions. *Nascap-2k* can be used to perform all four simulations of interest: (1) equilibrium space charge sheath; (2) “frozen ion” sheath; (3) dynamic PIC ions with fluid (Boltzmann or barometric) electrons (Hybrid PIC); (4) dynamic PIC ions and electrons (Full PIC). Previously we reported on one and three dimensional Full PIC calculations⁴ and Hybrid PIC calculations with prescribed potentials for a higher density plasma.⁵

This paper presents antenna simulations performed with *Nascap-2k*. The plasma is modeled using the hybrid PIC approach with PIC ions and fluid barometric electron densities. The plasma response, collected ion currents, and chassis floating potential are computed self-consistently with a near-square-wave bias applied to the antennas. Current limitation due to the thermal distribution of ions and the resulting angular momentum barrier are included. The different plasma response above and below the ion plasma frequency are shown.

In order to perform these calculations, *Nascap-2k*'s PIC capability has been expanded to include boundary injection and particle splitting. The boundary injection replaces particles that are either collected or leave the problem in long-running calculations. The particle splitting allows for modeling of the effects of the thermal distribution of velocities, as well as reducing particle size when passing into regions of finer resolution. The algorithms used for these capabilities along with their accuracy and limitations are discussed.

2 - PARTICLE IN CELL TECHNIQUES

Nascap-2k has primarily been used to model quasi-static phenomena. However, there are a large number of physical processes of interest whose timescales require a dynamic approach such as a particle-in-cell (PIC) technique. Examples of such processes are breakdown phenomena, plasma kinetics, and sheath structure about surfaces with potentials that change on a timescale comparable to the time it takes an ion to cross the sheath. PIC techniques can also be used to address problems in which analytic representations of the environmental currents are inadequate, such as in a spacecraft wake or in a cavity. A steady-state PIC technique, in which the ion space charge density is computed from macroparticles tracked from the boundary of the computational space until they are collected or exit the computation space, was successfully used to model the CHAWS experiment.⁶ In addition, PIC techniques can be useful when developing analytic models. In order to facilitate these modeling techniques, the ability to perform various types of PIC calculations was built into *Nascap-2k*. Recently, additional numeric techniques have been added to make two types of PIC calculations more flexible, robust, and faster—Hybrid PIC and Full PIC. In a Hybrid PIC calculation, the problem is initialized by creating ion macroparticles throughout the grid to represent a constant particle density. The ion macroparticles are tracked for one timestep and then volume potentials are computed using the resulting ion density and a barometric electron density.

$$\frac{\rho}{\epsilon_0} = \frac{\rho_i}{\epsilon_0} + \begin{cases} -(\phi + \theta)/\lambda^2 & \text{for } \phi > 0 \\ -(\theta/\lambda^2)\exp(\phi/\theta) & \text{for } \phi \leq 0 \end{cases}$$

where ϕ and θ are the plasma potential and temperature and λ is the debye length. The process is repeated for the time period of interest. In a Full PIC calculation both electron and ion macroparticles are tracked and volume potentials are computed using the resulting plasma density.

Two recent enhancements to *Nascap-2k*'s PIC capabilities are the injection of macroparticles from the boundary during a calculation and the splitting of the macroparticles.

In order to replace macroparticles that are collected by the probe or escape from the grid, it is necessary to periodically inject macroparticles from the boundary. This allows for the calculation of current for longer time periods. In hybrid PIC calculations without boundary injection, the low field region near the boundary of the problem develops a significant negative potential due to ion depletion. Boundary injection keeps these potentials near zero by replenishing the ions that have been collected or escaped.

Particle injection is implemented with an injection point at each quarter-boundary-surface-element. The injected particle has charge equal to the plasma thermal current times the area times the time interval and velocity equal to $\sqrt{\frac{2eT}{\pi m}}$, so that it represents the inbound half of the plasma density.

When the spacecraft is moving through the plasma this algorithm is modified to account for the motion. The current and velocity are computed in such a way that the density contribution of the injected particles varies from half the ion density for a stationary object to the full ion density for a high Mach number object.

Closely connected with boundary injection is macroparticle splitting. There are two major reasons for splitting macroparticles: one physical and one numeric. Even at moderate potentials, thermal effects can reduce collected currents. Some particles near the sheath edge have enough thermal velocity perpendicular to the electric field that angular momentum conservation prohibits collection. Particle splitting allows for a representation of the thermal distribution in the initial particle distribution and in particles injected from the boundary. From a numeric point of view, particle splitting can be used to keep the particle weight appropriate to the grid size and to help maintain the smoothness of the distribution. A large particle that originated in an outer grid is split in velocity in such a way that it preserves the plasma temperature and eventually becomes distributed over several volume elements in an inner grid.

Macroparticles may be split when they enter a more finely resolved region or when they are created either at the boundary or throughout the volume at problem initialization. The algorithm used is as follows:

1. Particles are split in velocity space only. Because high-field regions are often of interest, spatial splitting would raise problems with energy conservation.
2. Each particle carries a temperature, which is treated as isotropic. The fission products carry half the temperature of the original particle, while the remaining thermal energy appears as kinetic energy of the split particles. That each macroparticle has a temperature means that they can be split repeatedly, each time the particle enters a more finely resolved region.
3. For splitting purposes the Z-axis is defined to be along the direction of the particle velocity, the X-axis randomly chosen in the plane normal to Z, and the Y-axis mutually perpendicular.
4. Particles are split into two or three particles along each axis, except that a particle is not split along the Z-direction if the kinetic energy exceeds the thermal energy. Not splitting along Z helps avoid particle proliferation, but makes a small error by not preserving the original particle temperature along Z. Eight, nine, or twenty-seven new particles result.
5. Particle velocity is assumed to be acquired by acceleration rather than actual drift (i.e., spacecraft velocity). If there is actual drift, then the drift velocity is removed before splitting the particle and added back after.

6. If the particle is split by two along the X or Y axis, the new velocities are $\pm 0.707\sqrt{T/m}$. Along the Z axis the velocity increment is calculated as if the temperature were $T - 2\mu_0^2 \left(\sqrt{1 + \frac{T}{\mu_0^2}} - 1 \right)$.

7. If the particle is split by three along the X or Y axis, there is a zero-velocity central particle and two “probe” particles with velocity $\pm 0.866\sqrt{T/m}$. Along the Z axis the velocity increment is calculated as if the temperature were $T - 2\mu_0^2 \left(\sqrt{1 + \frac{T}{\mu_0^2}} - 1 \right)$.

The new particles have the same properties as the original particle except for velocity, weight (charge), and temperature.

3 - SELF-CONSISTENT ANTENNA CALCULATIONS

We performed a series of calculations of three-dimensional, time-dependent, self-consistent potentials and currents for a spacecraft with a VLF transmitting antenna. The *Nascap-2k* model used is shown in Figure 1 and Figure 2. The body is a 1.6 m aluminum cube and the two six-sided antennas are 0.05 m in diameter and 25 m long (3.75 m^2 each). The grid used for the calculations is shown in Figure 3 and Figure 4. The mesh unit of the outermost grid is 2 m.

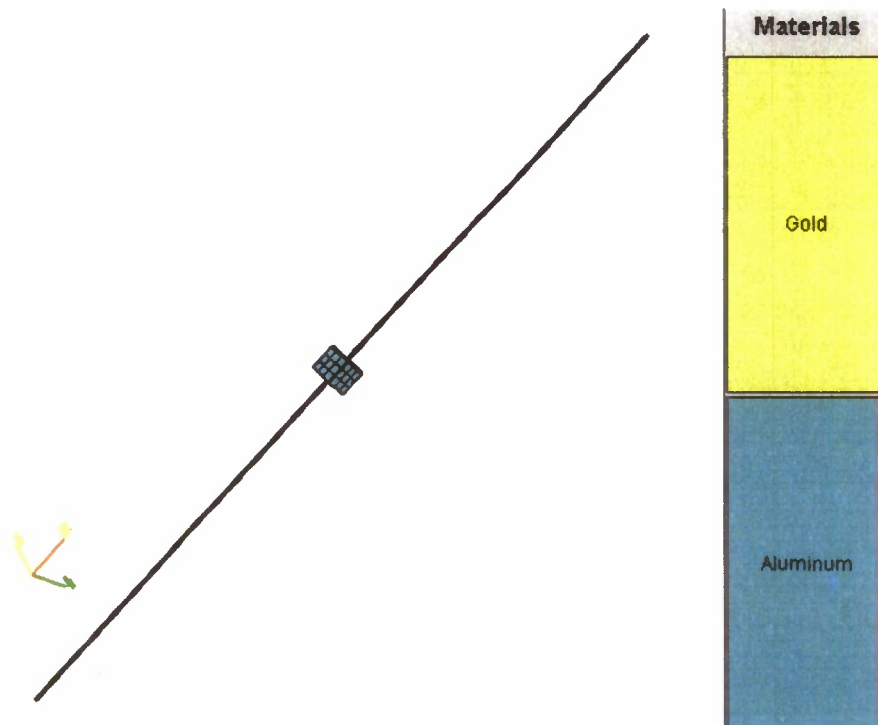


Figure 1. *Nascap-2k* model of VLF transmitting spacecraft.

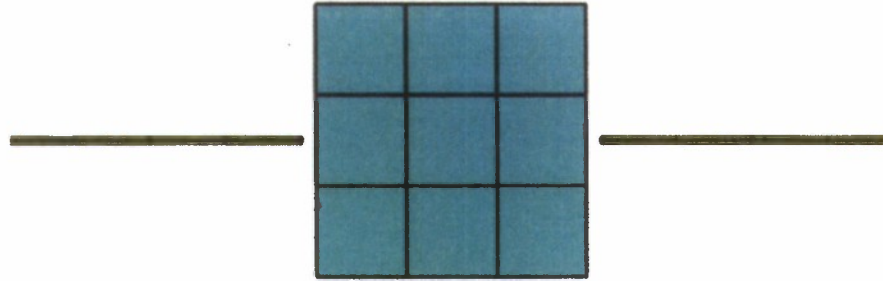


Figure 2. Expanded view of center portion of *Nascap-2k* model of VLF transmitting spacecraft.

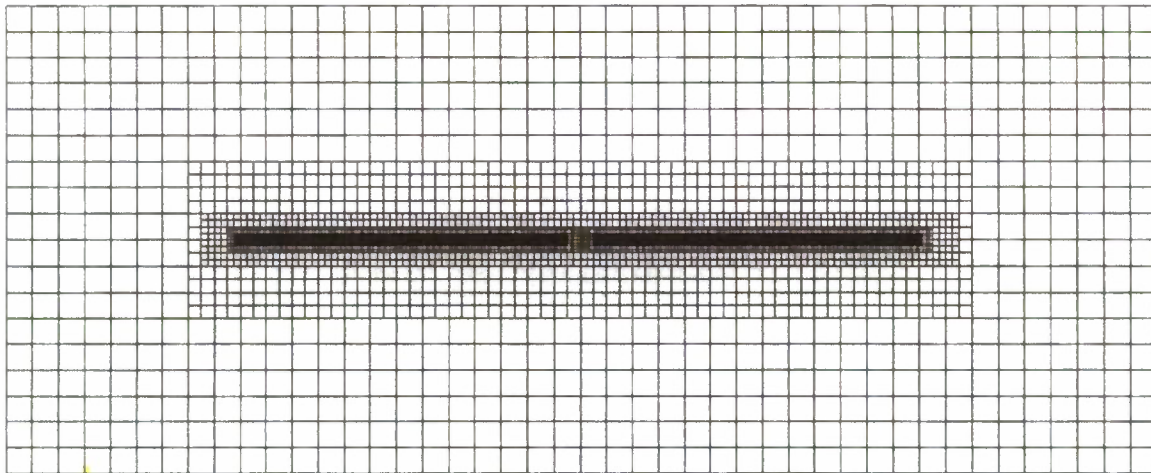


Figure 3. Grid used for VLF antenna calculations.

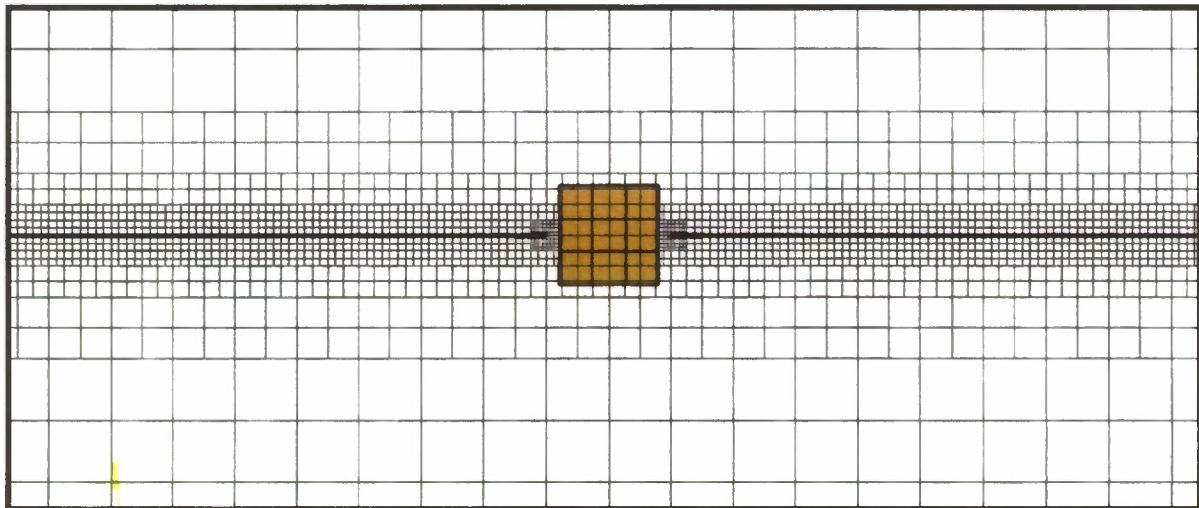


Figure 4. Close-up of center of grid used for antenna calculations.

Results from four calculations are shown below. The parameters of the calculations are shown in Table 1. In all cases, the potentials are adjusted to account for the incident current each timestep. The incident current is the tracked ion current together with an analytic electron current given by

$$I = \begin{cases} A j_{\text{th}} \exp(\phi/\theta) & \text{if } \phi \leq 0 \\ A j_{\text{th}} \left(1 + \frac{\phi}{\theta}\right) & \text{if } \phi > 0 \end{cases}$$

where A is the surface area and j_{th} is the plasma thermal current. One antenna is floating and the other has a variable bias with respect to the first. The aluminum box is floating. The timestep is set so that macroparticles move a reasonable distance each timestep. The Hybrid PIC charge density model is used.

The bias applied between the antenna elements is the sum of four Fourier components that approximates a square wave with amplitude of 1 kV and the indicated frequency, as shown in Figure 5. In the absence of plasma, each antenna element switches between ± 500 V. The square wave excitation is desirable in order to minimize time spent at low potentials, for which the plasma capacitance is highly variable. Having a phase-independent capacitance makes it easier to tune the power supply for optimal operation.

Table 1. Parameters used in antenna calculations.

| | Case 1 | Case 2 | Case 3 | Case 4 |
|-------------------------------------|----------------|--------------------|--------------------|----------------|
| Density (m^{-3}) | 10^8 | 10^8 | 10^9 | 10^9 |
| Temperature (eV) | 1 | 1 | 1 | H^+ |
| Species | H^+ | H^+ | H^+ | H^+ |
| Ion plasma frequency (kHz) | 2 | 2 | 6.6 | 6.6 |
| Frequency (kHz) | 10 | 10 | 12 | 2 |
| Splitting of initial macroparticles | None | All grids | All grids | All grids |
| Splitting on subgrid entry | None | Three levels | Three levels | Three levels |
| Macroparticle injection | None | Every 14 timesteps | Every 10 timesteps | Every timestep |
| Number of macroparticles (millions) | 0.50 | 3.9 to 13.1 | 3.9 to 10.4 | 2.9 to 12.2 |
| Current (mA) | 0.2 | 0.03 | 0.3 | 0.25 |
| Phase shift | $\sim 0^\circ$ | 10° | 12° | -7° |

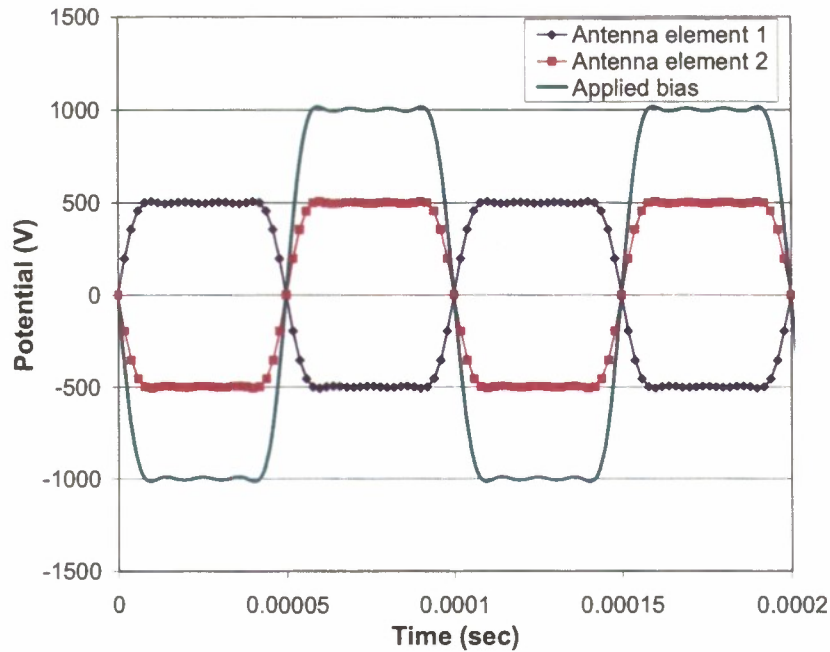


Figure 5. Applied bias values and resulting antenna potentials in the absence of a plasma.

The first two calculations are for tenuous plasma (10^8 m^{-3}) with excitation frequency well above the ion plasma frequency. Figure 6 shows the potential of the antenna elements and spacecraft body for Case 1, which has no particle splitting. In the initial few cycles the positive antenna element collects substantial electron current, driving the mean antenna potential to about -500 V. The spacecraft body initially follows this transient due to capacitive coupling, reaching negative potential of nearly 200 V, from which it gradually recovers. During the switching time from one polarity to the other there is a period during which both antenna elements are negative, and thus collecting some ions but no electrons. This causes the positive element to spike at positive potential following the switch, and the positive potential gradually decays during the half cycle.

Figure 7 shows the average surface current to an antenna element for the case with no particle splitting. As expected, the current is very noisy due to lack of splitting. It is also, at 0.2 mA ($50 \mu\text{A m}^{-2}$), much larger than the $2 \mu\text{A m}^{-2}$ orbit limited current for a cylinder accounting for the thermal angular momentum. This is as expected, since without splitting the thermal velocity distribution is not represented.

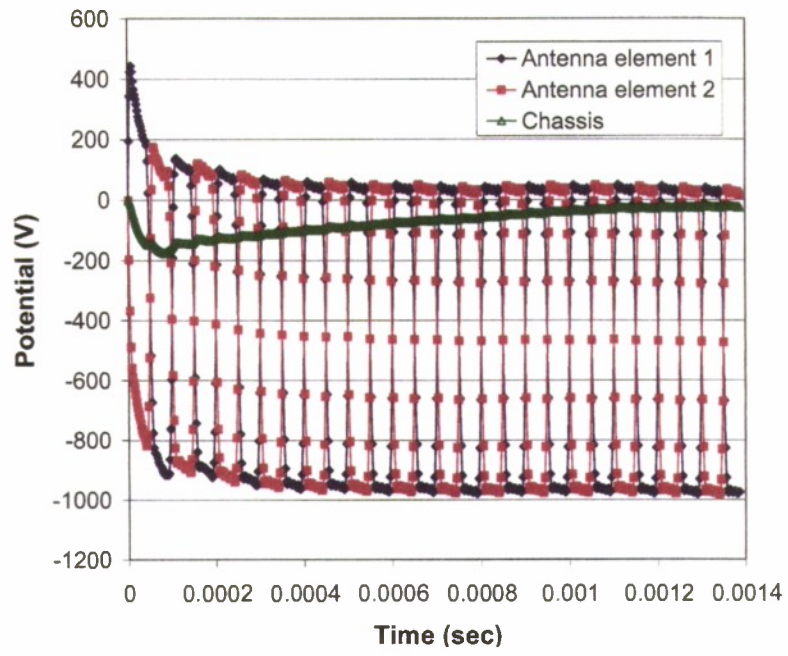


Figure 6. Time dependence of potentials for a 10^8 m^{-3} plasma at 10 kHz with no particle splitting (Case 1).

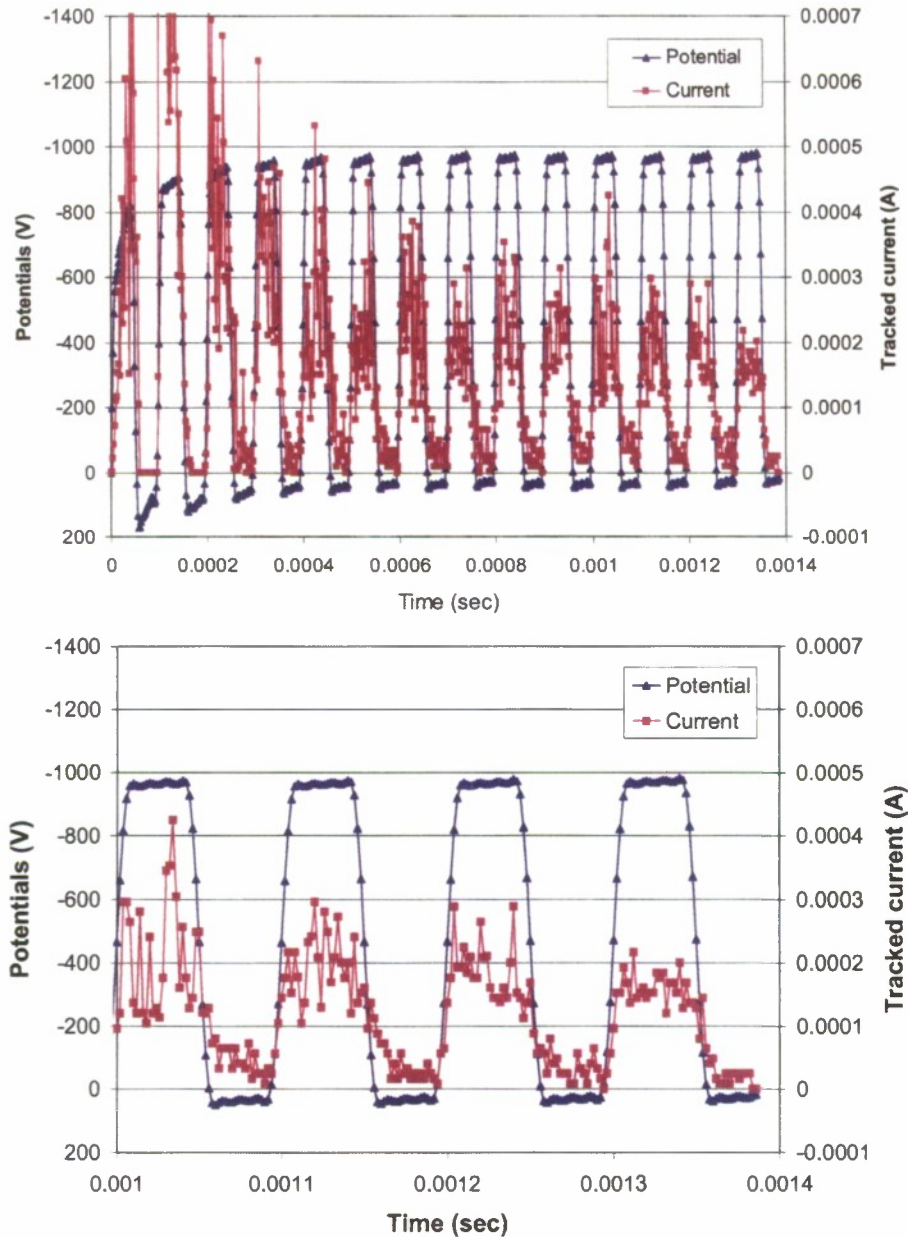


Figure 7. Potential and collected ion current of antenna element 2 for a 10^8 m^{-3} plasma at 10 kHz with no particle splitting (Case 1).

Case 2 has the same physical parameters as Case 1, but includes particle splitting, thus allowing both for smaller, more numerous particles and a representation of the thermal distribution. Figure 8 shows the potential distribution about the negative antenna element when fully biased at 2.11 ms, at the end of the simulation. At this low plasma density, the sheath nearly fills the grid and is more nearly spherical than cylindrical. The sheath also envelopes the positive antenna, providing a barrier to electrons, and thus allowing the system to float more positive than might be expected. (This barrier effect on electrons is not modeled in the present simulation.) The collected ion current, shown in Figure 9, is smoother, and by the end of the simulation has dropped to about $30 \mu\text{A}$ ($8 \mu\text{A m}^{-2}$), which is about four times orbit limited for a cylinder. This is reasonable because (1) the voltage is applied only half the time, and (2) additional current enters through the “end” of the sheath.

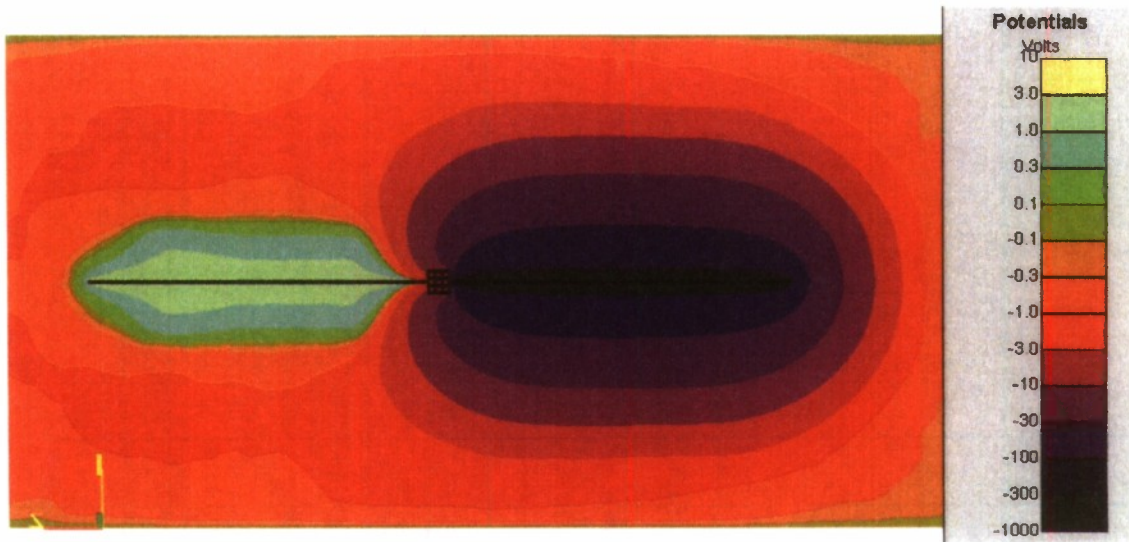


Figure 8. Potential structure in plane through center of spacecraft and antenna elements at 2.11 ms for a 10^8 m^{-3} plasma at 10 kHz (Case 2).

In both of the first two calculations, the plasma current to the negative antenna element responds almost immediately to the switch to negative potential, even though the applied frequency is well above the ion plasma frequency. This occurs because the applied electric fields are very high, and rapidly accelerate ions to speeds far in excess of their thermal velocity. However, the response to the positive switch is less sudden, and ions continue to be collected by the positive antenna element through nearly all its positive half-cycle. The fundamental frequency component of the current lags the applied voltage by a 10° phase shift, substantially less than the ninety degree shift expected in the linear regime.

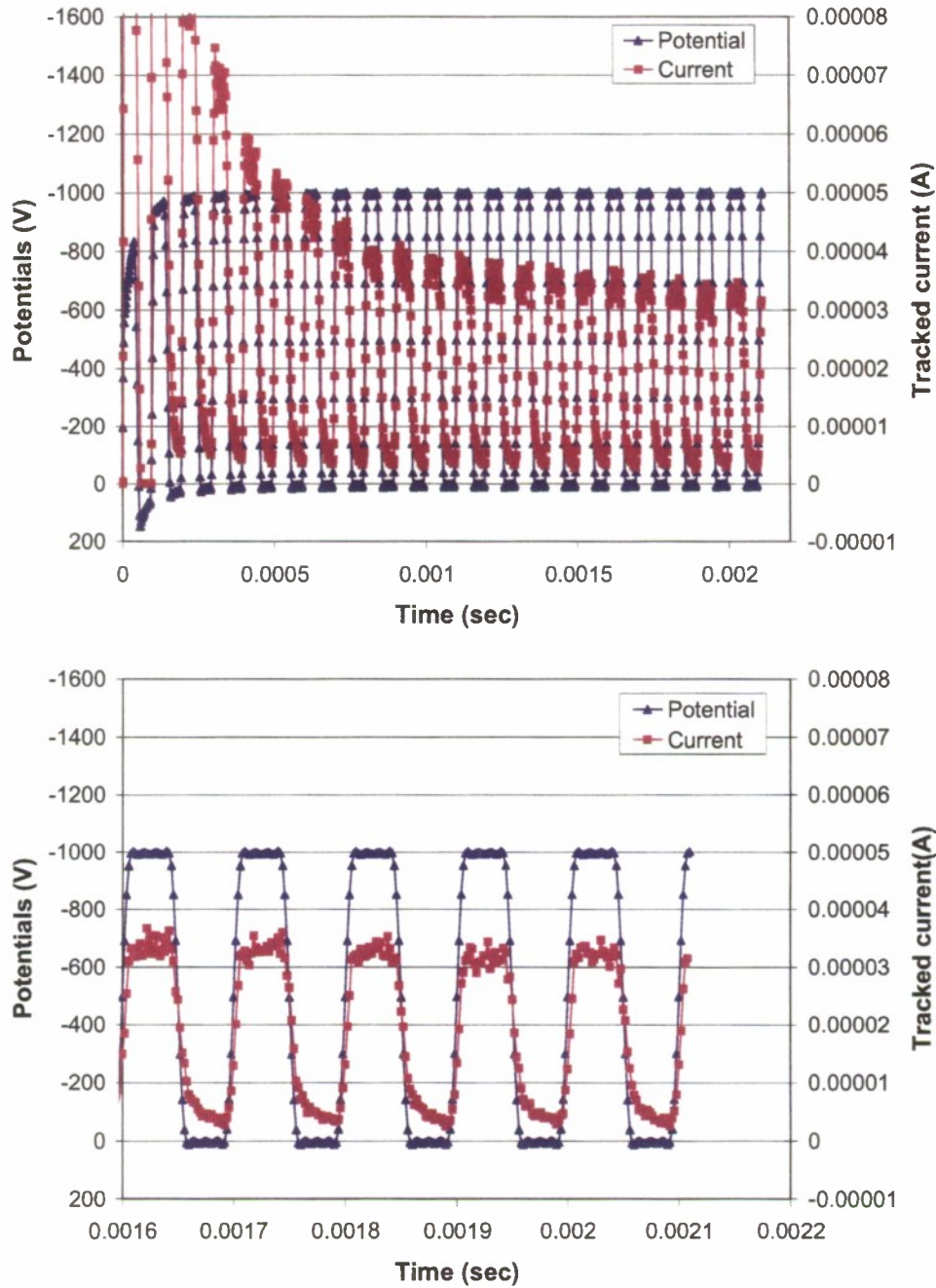


Figure 9. Potential and collected ion current of antenna element 2 for a 10^8 m^{-3} plasma at 10 kHz (Case 2).

Cases 3 and 4, at high and low frequency with respect to the ion plasma frequency, treat a plasma that is an order of magnitude more dense (10^9 m^{-3}) than the first two calculations, and thus has a considerably smaller sheath (Figure 10). The sheath is much more cylindrical in character than at lower density (Figure 8), but the spherelike end cap sheath remains substantial. (Noise in the background plasma shown in Figure 10 is at the 1 V level.) The antenna and spacecraft potentials (Figure 11) follow very much the same pattern as the more tenuous plasma (Figure 6), except that the positive potentials are better held in check by the higher electron current. Similar to the previous cases, a positive spike in potential is seen on switching. The current is 0.2 to 0.3 mA ($80 \mu\text{A m}^{-2}$), which is four times $20 \mu\text{A m}^{-2}$, the orbit limited value for a cylinder in this plasma, and far less than

the spherical orbit limited value of $600 \mu\text{A m}^{-2}$. The current variation over a cycle reaches repeating on the fifth cycle at 12 kHz and on the third cycle at 2 kHz. The current variation with time (Figure 12 and Figure 13) differs between the high and low frequency cases. Both show an initial rapid increase as ions within the sheath are collected. In the high frequency case (Figure 12) a further gradual increase occurs as ions near the sheath edge, which take longer to reach the antenna, are collected. The fundamental frequency component of the current lags the applied voltage by a 12° phase shift, more than that seen in the lower density case. In the low frequency case (Figure 13) all ions within the sheath are exhausted early in the pulse, and the collected current is limited to those ions eroded from the sheath edge during the pulse, resulting in decreasing current during most of the cycle. Consequently, the fundamental frequency component of the current leads the applied voltage by a phase shift of about 7° .

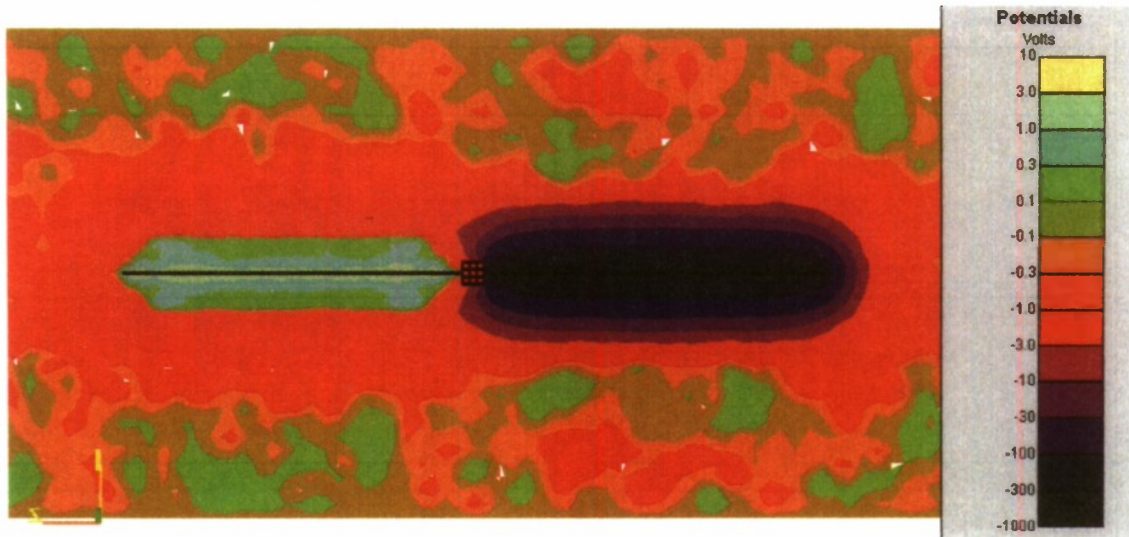


Figure 10. Potential structure in plane through center of spacecraft and antenna arms at 1.34 ms for the high density 10^9 m^{-3} plasma at 12 kHz (Case 3).

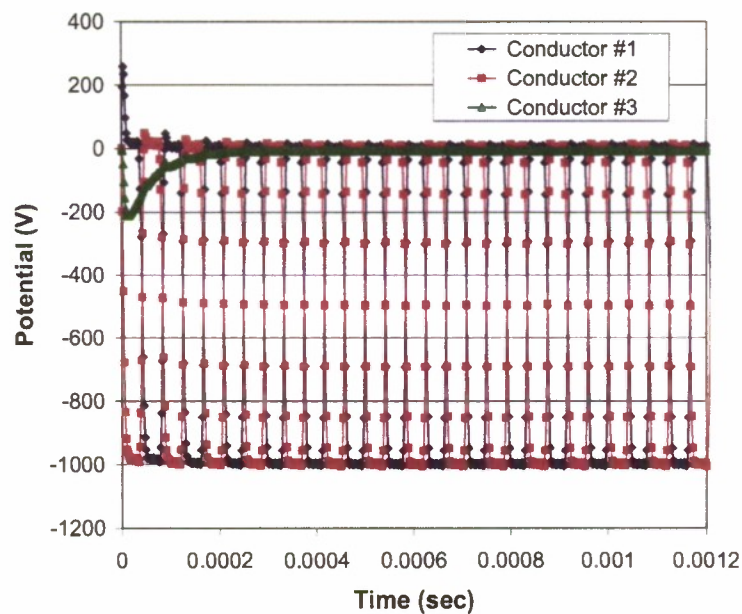


Figure 11. Time dependence of potentials for the high density 10^9 m^{-3} plasma at 12 kHz (Case 3).

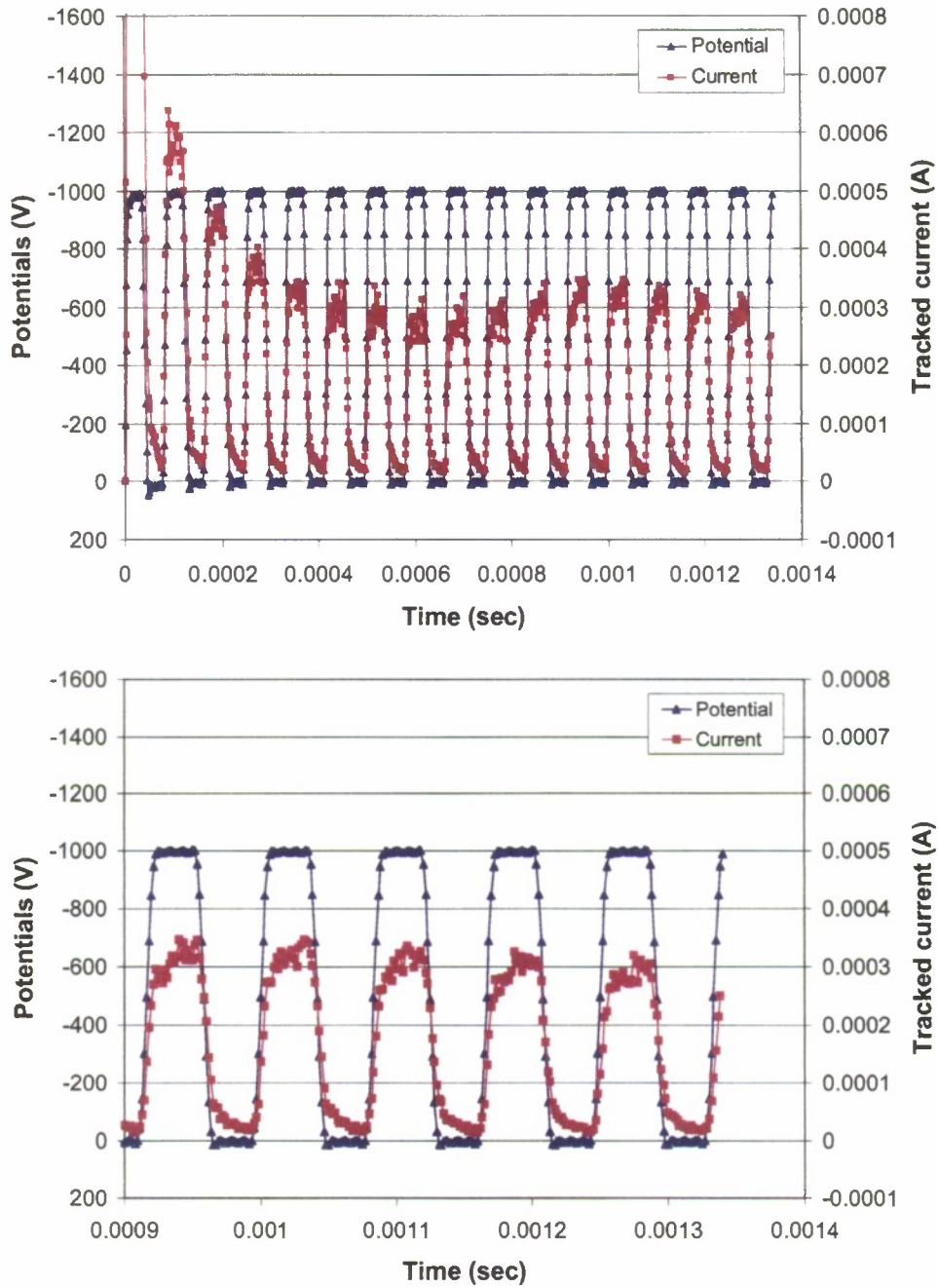


Figure 12. Potential and collected ion current of antenna element 2 for the high density 10^9 m^{-3} plasma at 12 kHz (Case 3). Note that the current lags the potential by a 12° phase shift.

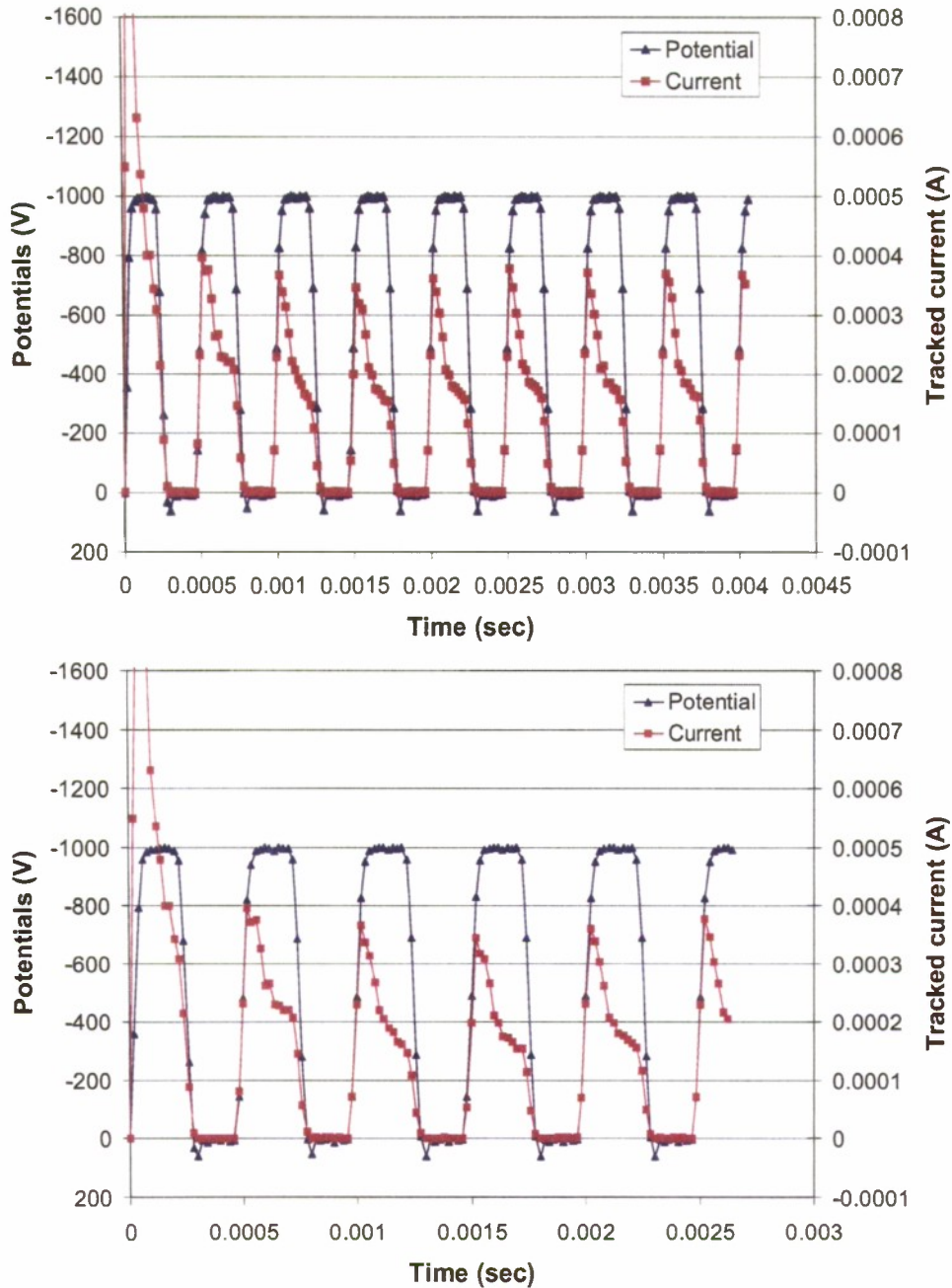


Figure 13. Potential and collected ion current of antenna element 2 for the high density 10^9 m^{-3} plasma at 2 kHz (Case 4). Note that the current leads the potential by a phase shift of about 7° .

Figure 14 illustrates the difference between the high and low frequency behavior. It shows the results of a one-dimensional calculation of a spherical antenna in a plasma of density $4 \times 10^7 \text{ m}^{-3}$ with applied sinusoidal potential of 5000V at 10 kHz (left) and 1 kHz (right). At high frequency the sheath (defined as the region from which electrons are excluded) extends far into the ambient plasma, and ions are collected only from the inner region of the sheath. The collected current can increase during the time the potential is applied as ions are collected from progressively farther out in the sheath at each cycle. By contrast, at low frequency the sheath region is nearly emptied at each cycle, so that the current must fall off as ions from the sheath edge region are difficult to collect.

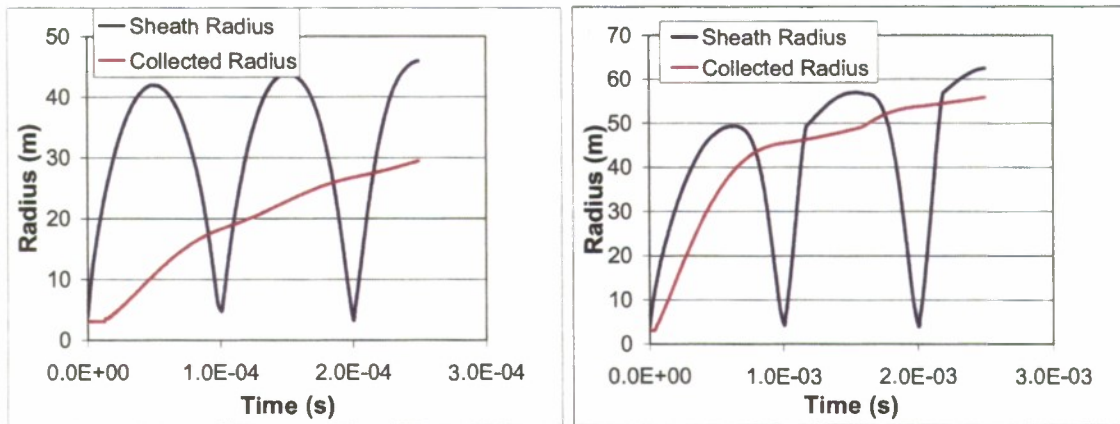


Figure 14. One dimensional spherical calculation of sheath radius and ion collection radius at high frequency (left) and low frequency (right).

4 - CONCLUSIONS

We have used *Nascap-2k* to study the plasma interactions of a high voltage near-square-wave VLF antenna in MEO plasma. The model consists of two 25 meter antenna elements biased ± 1000 V at voltages above or below the ion plasma frequency. For these very high applied voltages, the plasma response is nonlinear, and the sheaths are more spherical than cylindrical, especially at the lower density. In modeling the system it is important to use particle splitting and injection techniques that replenish depleted plasma at boundaries, maintain appropriately sized macroparticles, and provide a reasonable representation of the plasma thermal distribution. When this is done, the incident current is in reasonable agreement with orbit-limited predictions.

When the excitation frequency is above the ion plasma frequency the plasma current to an antenna element increases sharply when the potential is applied, and falls off relatively slowly when it is removed, with incident ion current continuing substantially into the unbiased half-cycle. Below the ion plasma frequency the ion current peaks sharply when the potential is applied, falls off substantially during the half-cycle, and drops sharply to zero when the potential is removed. The difference can be understood in terms of the sheath being depleted of ions within every cycle at low frequency, but not at high frequency. The current lags the applied voltage for excitation frequencies above the ion plasma frequency by 10° at the low density and 12° at the high density, which is much less than the ninety degree shift expected in the linear regime. At low frequency (calculated for the high density only) the current leads the applied voltage by 7° .

ACKNOWLEDGEMENTS

This paper was prepared with funding from the Air Force Research Laboratory.

REFERENCES

- [1] Vampola, A. L., and G. A. Kuck, Induced precipitation of inner zone electrons, 1, Observations, *J Geophys Res*, 83, 2543, 1978.
- [2] Imhof, W. L., E. E. Gaines, J. B. Reagan, Evidence for the resonance precipitation of energetic electrons from the slot region of the radiation belts, *J Geophys Res*, 79, 3141, 1974.
- [3] Inan, U. S., H. C. Chang, R. A. Helliwell, Electron precipitation zones around major ground-based VLF signal sources, *J Geophys Res*, 89, 2891, 1984.
- [4] M.J. Mandell, D.L. Cooke, Nascap-2k as a PIC Code, *Proceedings of the 8th Spacecraft Charging Technology Conference*, Huntsville, AL, NASA/CP-2004-213091, 2003.
- [5] M.J. Mandell, V.A. Davis, D.L. Cooke, A.T. Wheelock, C.J. Roth, Nascap-2k simulations of a VLF plasma antenna, *Proceedings of the 9th Spacecraft Charging Conference*, Tsukuba, Japan, Japan Aerospace Exploration Agency (JAXA), 2005.
- [6] V.A. Davis, M.J. Mandell, D.L. Cooke, and C.L. Enloe, High-voltage interactions in plasma wakes: Simulation and flight measurements from the Charge Hazards and Wake Studies (CHAWS) experiment, *J Geophys Res*, 104, A6, p. 12445, 1999.